Melt Growth of Semiconductor Crystals Under Microgravity

Zhigang Yin, Xingwang Zhang, Wei Wang, Xiaoya Li and Jianding Yu

Abstract The low-gravity environment aboard the space offers an advanced platform to prepare materials with improved properties as compared with their terrestrial counterparts, and allows an in-depth understanding of crystal-growth-related phenomena that are masked by gravity on the earth. The main achievements in the melt growth of semiconductors under microgravity are listed below: (i) on the way towards high-quality semiconductors with chemical homogeneities on both the macroscopic and microscopic scales, the dependence of solute transport on the buoyancy-driven convection and Marangoni convection was better understood; (ii) the underlying mechanism of detached Bridgman growth was clarified based on the microgravity experiments, which in turn guided the ground-based crystal growth processes; (iii) new crystal growth techniques including the traveling liquidus-zone method and the vertical gradient freezing method were proposed and developed, and chemically homogeneous semiconductor alloys such as $Ge_{1-x}Si_x$ and $In_xGa_{1-x}Sb$ were successfully grown using these methods under microgravity. In this part, the main progresses in these areas are reviewed and summarized.

Keywords Microgravity growth · Semiconductor · Detached growth · Buoyancy-driven convection

Z. Yin (✉) · X. Zhang (✉)
Key Lab of Semiconductor Materials Science, Institute of Semiconductors, Chinese Academy of Sciences, Beijing 100083, China

College of Materials Science and Opto-Electronic Technology, University of Chinese Academy of Sciences, Beijing 100049, China

Z. Yin
e-mail: yzhg@semi.ac.cn

X. Zhang
e-mail: xwzhang@semi.ac.cn

W. Wang · X. Li · J. Yu
State Key Lab of High Performance Ceramics and Superfine Microstructure, Shanghai Institute of Ceramics, Chinese Academy of Sciences, Shanghai 200050, China

W. R. Hu and Q. Kang (eds.), *Physical Science Under Microgravity: Experiments on Board the SJ-10 Recoverable Satellite*, Research for Development,
https://doi.org/10.1007/978-981-13-1340-0_13

1 Introduction

The progress in space technology provides new opportunities for materials research. The first crystal growth experiment performed during the Apollo emissions in the late 1960s announced the birth of space materials science [1]. The unique microgravity environment in space offers a new degree of freedom for materials processing, allowing in-depth insights into the fundamental issues in crystal growth. Investigations in this field mainly aim at the following three goals:

(i) Manufacturing perfect crystals with properties that cannot be obtained on the earth by eliminating the influence of gravity. An exemplified example is that the space-grown GaAs semi-insulating crystals are featured with improved stoichiometry and lower defect concentration, and the field effect transistors fabricated based on these crystals have performances much better than the terrestrial samples [2, 3].

(ii) Understanding fundamental phenomena that are masked by gravity and therefore are difficult to study quantitatively on the earth. For instance, fluids are affected by buoyancy-driven convection, and microgravity helps isolating such effect from the targeted systems [4].

(iii) Improving the ground-based crystal growth. An excellent example is the understanding of the underlying mechanism of detached directional solidification and its guidance to the terrestrial preparations. The detached growth on the earth greatly reduces the dislocation densities of the crystals and provides new opportunities for their device applications [5].

Space materials science covers the whole materials family, and the preparations of metals, semiconductors, and biological materials, are all intensively studied under microgravity. In this review, we only limit our scope in semiconductors. Different growth techniques, including melt-related methods (floating zone method and Bridgman solidification), solution-based routes (liquid epitaxy and traveling heater method with solution starting materials), and chemical or physical vapor deposition were employed in experiments aboard spacecraft. Melt growth is the most widely exploited technique to produce high-quality, single-crystalline semiconductor chips for commercial applications. Among the melt growth methods, Bridgman directional solidification is the main-stream technique for microgravity semiconductor crystal growth. The main advantage of Bridgman growth as compared with other crystal growth techniques is its simplicity. Typically, the ampoule structure used in Bridgman method is easily modified to fix the charges along both the axial and radial directions. Such a characteristic is highly attractive for the microgravity experiments, taking into account the harsh mechanical environment during the spacecraft emission. The Bridgman method involves heating a polycrystalline material in a crucible above its melting point and then slowly cooling it from one end where the seed crystal locates. During this process, single crystal is progressively formed along the axial direction of the initial ingot. Bridgman solidification can be performed under horizontal or vertical geometries, and the latter is dominant in the reported experiments.

We mainly focus on the progresses of the melt growth of semiconductor crystals under microgravity, and special attention is paid to the Bridgman solidification and related issues. The review is divided into four parts: in part I, the studies towards chemically homogeneous semiconductors both macroscopically and microscopically are reviewed, and the difficulties and recent progresses are introduced; part II introduces the new understandings on detached solidification, a phenomenon found 40 years ago, and its guidance to the terrestrial materials research are discussed; in part III we introduce the emerging crystal growth concepts, including the traveling-liquidus zone method and the vertical gradient freezing method, and the efforts towards high-quality binary or ternary semiconductor alloys by using these methods are also discussed; part IV is a summary of this review.

2 Towards Diffusion-Controlled Growth

2.1 Segregation and Solute Transport Under Microgravity

According to the classical Tiller's theory, steady-state growth can be achieved on condition that the convective mixing is negligible and the solute transport is dominated by diffusion [6]. The initial transient that follows the Tiller's theory can be expressed as [7]

$$C_s(x)/C_0 = k + (1-k)\left[1 - \exp\left(-kRx/D\right)\right] \tag{1}$$

where $C_s(x)$ is the dopant concentration in the solid at a distance x from beginning of the sample, C_0 is the uniform concentration of the initial melt, k is the equilibrium distribution coefficient, D is the diffusion coefficient of the solute in the melt, and R is the growth rate. Steady growth can occur only if the growth rate R is fixed and the impurity concentration adjacent to the interface remains constant. These conditions are not satisfied during the ground-based normal freezing because of the buoyancy-driven convection, while space provides an ideal platform to achieve the steady-state crystal growth. Without the perturbation by buoyancy-induced convection, diffusive transport can be obtained in the melt and therefore, after a short initial time, the crystals should have a uniform chemical composition.

In an early work performed by Witt et al., a steady-state growth was really observed in the Te-doped InSb crystals grown by Bridgman method on Skylab spacecraft [8]. A uniform axial distribution of Te was obtained across the entire grown crystal, as evidenced by both Hall-effect measurements and ion-microprobe scanning. Thermoelectric semiconductor crystal of $Bi_2Te_{2.79}Se_{0.21}$ was grown by Zhou et al. on the Russian Foton-M3 spacecraft, and EPMA analysis show that the axial composition is more homogeneous than that of the ground-based crystal [9]. Diffusion-controlled growth was also found in Ge crystals grown by Bridgman technique and homogeneous composition distribution along the axial direction was

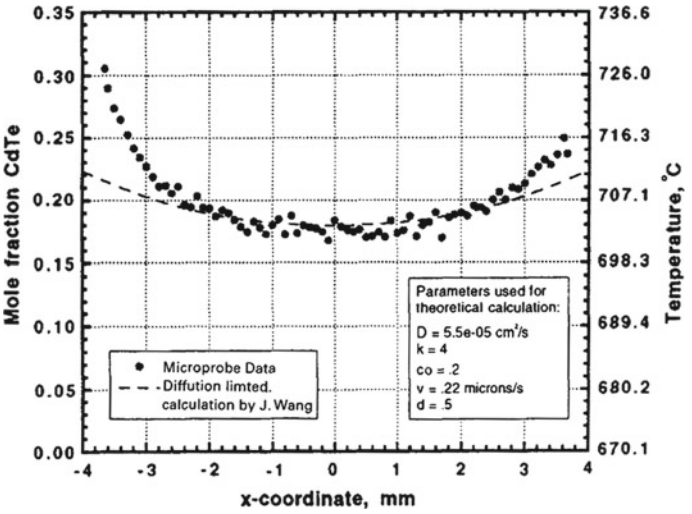

Fig. 1 Radial composition profile of HgCdTe crystal; the dashed line indicates the calculated results according to the diffusion-controlled scheme. Reprinted with permission from reference [12]

achieved [10]. However, notable radial segregation was observed in the sample. Bly et al. also found that the axial Se distribution for the space-grown Se-doped GaAs is diffusion-limited, whereas an evident radial segregation is present in the crystal [11]. Similarly, the axial compositional profile of space-based HgCdTe crystal agrees well with the diffusion-controlled scenario while the radial distribution not (see Fig. 1) [12]. Although uniform axial composition distribution can be achieved, researchers always fail in producing diffusion-limited radial composition profiles.

All these studies inform that the crystal growth performed in space cannot be simply treated as a process in which convection is absent. Although the gravity level in spacecraft is significantly lower than that on the earth, it is not zero. To explain the observed experimental results, residual accelerations should be considered. Residual accelerations on spacecraft are mainly composed of two categories—quasi-static and vibrational accelerations [13]. The magnitude and direction of the quasi-static accelerations are determined by the orbit altitude and the orientation of spacecraft axes with respect to the earth. In most cases, the residual quasi-static accelerations in the spacecraft are on the order of 10^{-4} to 10^{-6} g_0 (g_0: the gravitational acceleration on the earth) with frequencies below 0.01 Hz. The vibrational accelerations (also called g-jitter) are mainly originated from the elastic vibrations of the spacecraft, thruster firings for orbital correction, daily crew activities, and active machinery and so on. In general, the vibrational component frequencies range from 0.01 to 300 Hz and the amplitude can be as high as 10^{-2} g_0 (e.g., during orbital adjustment). In order to fabricate homogeneous semiconductor crystals, particular attention should be paid on the residual accelerations. For example, Alexander et al. reported that the vibrational accelerations recorded by spacecraft accelerometers have a strong influence on the

solidifying system, and a close correlation between the vibrational accelerations and the disturbances in the transport conditions were clearly resolved [14].

We now discuss the different segregation behaviors along the axial and radial directions for crystals grown under microgravity. The convective flows induced by residual gravity mix the melt and cause fluctuations in the axial and radial segregation of solute. As discussed by Brown et al., the degree of melt mixing can be categorized into three cases: no mixing, poor mixing and strong mixing [13]. For the axial case, the effective segregation coefficient (k_{eff}) is nearly unity, suggesting a negligible segregation at the no mixing condition; k_{eff} gradually deviates from unity with the enhancing flow intensity, and eventually approaches the equilibrium distribution coefficient (k) as a result the full mixing of the diffusion layer with the melt (strong mixing). Similarly, a nearly uniform radial composition distribution is predicted in both the no mixing and strong mixing conditions. A uniqueness of the radial segregation is that it does not vary monotonically with the flow intensity. As nontrivial cellular convection appears in the melt, it interferes with the diffusion layer adjacent to the growth interface and causes a drastic variation of the radial composition [13, 15]. This corresponds to the poor mixing condition. For many of the space crystal growth experiments, the residual accelerations induce non-negligible convective flows which produce a poor mixing condition. These discussions explain why the space growth experiments usually yield an improvement of axial segregation and a deterioration of radial composition distribution.

Intensive numerical modeling works focused on the microgravity growth of semiconductors from melts were performed by various groups, in order to achieve better understandings of the experimental results and offer guides for the modified experimental designs. Griffin et al. investigated the influence of temporal variations in the gravity magnitude on the natural convection during the Bridgman solidification of semiconductors [16]. The results show that for low Rayleigh numbers the response time to step changes in g is controlled by the momentum diffusive time scale, while for higher Rayleigh numbers the response time is reduced due to the inertial effects. Alexander and coworkers investigated the effect of quasi-static and vibrational accelerations on the dopant distributions, and found that the composition non-uniformity is strongly dependent on the orientation of quasi-static acceleration. Moreover, they pointed that the influence of vibrational acceleration can last for thousands of seconds after the termination of the pulse [17]. Naumann developed an analytical model for the two-dimensional flow field to examine the effects of small residual accelerations [18]. He found that the quasi-static and vibrational accelerations on the order of $10^{-4}g_0$ can induce severe solute redistribution, and orientating the furnace axis along the residual gravity vector can ameliorate this effect.

Derby and coworkers developed a three-dimensional (3D) method to model the vertical Bridgman growth which incorporates melt convection, heat transfer, segregation, and solidification related phenomena in the crucible [19]. By implementing the deforming-grid, front-tracking method, they built a framework in which the 3D shape and movement of the crystal-melt interface is represented. They developed a Galerkin mixed-order formulation which employs a higher-order, quadratic representation of the velocity field with a linear, discontinuous basis to meet the challenges

to produce robust, accurate solutions for incompressible 3D flows. The boundary conditions can be supplied in a self-consistent way by coupling another furnace-scale model which deals with heat transfer by radiation and conduction. These methods have been successfully used to compute the growth of CdZnTe [20, 21].

Most of the experimental works performed the Bridgman technique is based on diluted systems. The Duffar group focused on the growth of concentrated semiconductors and used GaInSb as a model system [22, 23]. The ground-based experiments show that the considerable chemical segregation which is coupled with thermosolutal convection results in huge deformations of the crystal-melt interface, and the resultant interface curvature can exceed the crystal diameter [23]. A semi-empirical analytical expression was developed to account for the evolution of the interface deflection during the growth, and the results show that low pulling rate and low thermal deflection favors for achieving flat growth interface [24]. The axial indium component distribution for the space-grown crystal exhibits a Scheil-like solute profile apart from the beginning of the solidification. To understand this puzzling result, theoretical simulations were performed by Stelian et al. and based on the results they proposed an experimental scheme to improve the chemical homogeneity [25]. Moreover, the influence of g-jitter on the chemical segregation was also simulated by varying its amplitude and frequency [26]. The results show that low-frequency ($<10^{-2}$ Hz) residual gravity have a noticeable influence whereas the crystal growth can tolerate the high-frequency g-jitters.

2.2 Influence of Marangoni Convection

Another source that contributes to the considerable segregation under microgravity is Marangoni convection, which is usually masked on ground-based crystal growth due to the strong buoyancy-driven flow. According to its surface-related nature, it is difficult to study the Marangoni convection and related phenomena in a quantitative way. Nakamura et al. developed an in situ visualization system to investigate the Marangoni convection in a molten silicon bridge, and comparative studies on ground- and space-based experiments were performed [27]. Such a method is also applicable to other semiconductor molten systems. Two types of temperature oscillation were observed in the microgravity experiment in the molten silicon, in which one is featured with a frequency of about 0.1 Hz and the other has no remarkable frequency. The former oscillation has an antiphase correlation in thermocouples with 90° separation in azimuthal angle, while the latter is characterized by an antiphase correlation with 180° azimuthal angle separation. The Marangoni number (Ma) was extracted by carefully measuring the temperature fluctuations, and a value of 1900 was determined for the microgravity condition [28]. In a recent study, the critical temperature difference and the critical Marangoni number (Ma_{c2}) which are needed for the occurrence of oscillate flow are determined in a rather wide range of aspect ratio [29].

Due to its connection with the occurrence of free surface, Marangoni convection is prevalent in the floating zone growth experiments [13]. For the Bridgman growth case, Marangoni convection can also play an important role in the heat and solute transportation, when free surface appears. For example, considerable chemical segregation of Te in Te-doped GaSb has been observed along the axial direction for the space-grown samples, demonstrating a strong mixing of the melt during the whole growth process [30]. The influence of residual gravity during the experiments is effectively controlled and it cannot account for the observed macroscopic segregation. This conclusion is corroborated by numerical studies in which the extracted velocity field is in good agreement with the strong disturbance of solutal boundary layer close to the solid-liquid interface [30]. Mathematical simulations confirm that as the buoyancy-induced convection is reduced, the intensity of convective flow is completely determined by the Marangoni convection [13]. Under microgravity, the velocity of convective flow near the solid-liquid interface can reach a value as high as 0.5 cm/s even at a small radial temperature gradient of 1.2 K/cm [13]. Such a strong convection flow is comparable with the conventional level of the pure-buoyancy-dominated case on ground. As a result, it is hard to achieve chemical homogeneity under microgravity when free surface is present.

Marangoni convection not only results in macrosegregation, but also leads to microsegregation—microscopic variations of the dopant concentration (dopant striations). It is known that the Rayleigh number, which is a measure of the driving force for buoyancy convection is reduced by a factor of 10^4 to 10^6 under microgravity, depending on the residual gravity level [31]. Moreover, it was revealed that, the magnitude of vibrational accelerations only slightly influences the convective flows near the growth interface in the absence of Marangoni convection. A close examination of the ground-based Ge:Ga growth shows that on a closed melt surface, the vibrational effects do not yield noticeable striations even at amplitudes of 2×10^{-1} g_0 [13]. An extrapolation to the microgravity condition yields an upper limit (at which striations are absent) of vibrational acceleration of $\sim 2 \times 10^{-3} g_0$ [13]. Therefore, the residual gravity and the resultant buoyancy-driven convection do no play a role in the striation formation as important as Marangoni convection. Obviously, the reported striations by various groups for the space-based crystals are mainly caused by unsteady (or oscillatory) Marangoni convections. The unsteady Marangoni convection is characterized by the temperature variations in the melt near the growth interface, which gives rise to the variations in the growth rate and the resultant local inhomogeneity. For example, Schweizer and coworkers found that under temperature fluctuations of 0.5–0.7 °C with a frequency range <0.5 Hz, the microscopic growth rate fluctuates significantly around the average growth rate of 1 mm/min [32]. Growth rates up to 4, ~0 mm/min, and negative values were all observed in the experiments. Dopant striations are clearly visible from the obtained crystals, as shown in Fig. 2.

It is the low Prandtl number (*Pr*, defined as the ratio between the fluid kinematic viscosity and the thermal diffusivity) of semiconductor melt that results in the easy formation of striations during the semiconductor crystal growth [33, 34]. As revealed by 3D numerical simulations, Ma_{c2}, which determines the onset of time-dependent convection is strongly dependent on *Pr* [34]. For low-*Pr* melts, the

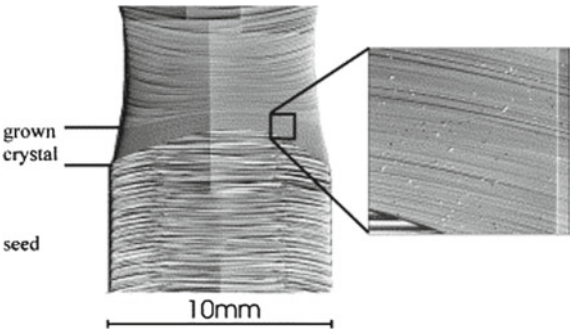

Fig. 2 Micrograph of the etched μg crystal of Si, in which dopant striations induced by Marangoni convection are clearly visible. Reprinted with permission from reference [32]

steady-to-unsteady transition is mainly caused by the inertial effect [35]. Microgravity provides an ideal platform to accurately determine the parameter of Ma_{c2} for various semiconductor melts. For example, Cröll et al. have carefully investigated the critical Marangoni number of GaSb and obtained a Ma_{c2} of 375 ± 125 from the striation to non-striation transition [37]. Such a value is in good agreement with 3D numerical simulations which yields $Ma_{c2} = 355 \pm 90$. Their experiments were performed during the German-Canadian Spacelab-4 mission with a GaSb ingot diameter up to 15 mm. For Si and GaAs melts, the Ma_{c2} values are 150 ± 50 and ~400, respectively [36]. Based on these data obtained by space experiments, the values of Ma_{c2} for semiconductor melts can be expressed empirically as

$$Ma_{c2} = 2.2 \times 10^4 Pr^{1.32} \tag{2}$$

Taking into account the difficulties in measuring Ma_{c2} for all the semiconductor melts, this emprical formula extracted by data fitting is very useful for predicting the onset of steady-unsteady transition of a given melt.

The driving force for Marangoni convection is proportional to the local thermal gradient or component gradient at the free surface. Therefore, reducing these gradients at the free surface seems to be a powerful way to eliminate or ameliorate the influence of microsegregation. However, for a true crystal growth process, there leaves no enough room to tune these parameters. For instance, a smaller thermal gradient results in a more deformed interface shape, although it can considerably reduce the convection level. On the other hand, according to classical theory, the steady diffusion-controlled growth yields a non-zero solute gradient near the growth interface. Here we note that the occurrence of free surface on microgravity condition is not necessarily associated with the formation of dopant striations, even when the Marangoni number exceeds the critical value of Ma_{c2}. GaSb crystal growth was conducted on the scientific platform of Chinese recoverable satellite and a notable diameter shrinkage of the crystal was observed [37]. The longitudinal cross-section characterizations of the crystal do not resolve any growth striations, indicating no unsteady Marangoni convection was involved in the growth. The GaSb growth free of Marangoni convection is, in a rather possibility, associated with the formation

of a thin oxide layer surrounding the crystal [37]. Another work also highlights the role of thin oxide layer in suppressing the Marangoni convection [38]. These observations provide a possible means to suppress the occurrence of impurity striation and improve the quality of the grown crystals.

2.3 Damping the Convections Under Microgravity

Both the experimental observations and numerical simulations indicate that the growth of semiconductors under the microgravity environment is still influenced by the buoyancy-induced convection. It has long been anticipated that the application of a static magnetic field during the growth can dampen the convective flow in the melt. This idea works in principle for the semiconductor systems since most of the semiconductors are good conductors in their melt states. However, to suppress the convection to the diffusion-controlled level on the earth, the applied magnetic field should be as high as a few Tesla or even larger [39–41]. Such a large magnetic field results in a rather high energy consumption and is not economically acceptable. Furthermore, a strong magnetic field is commonly associated with non-negligible, additional effects like thermoelectric convection [41, 42]. Combining the microgravity with the magnetic field seems to be a more effective way to dampen the buoyancy-driven convection to the desired level and produce the pure diffusion-controlled growth.

Many groups have explored the possibility of applying magnetic field during the semiconductor crystal growth. Fripp et al. performed numerical simulations for the microgravity growth of PbSnTe using the vertical Bridgman configuration, in which an axial magnetic field is applied to interfere with radial convection component [43]. Their results show that the applied magnetic field is very effective in controlling the convective flow, and a moderate axial magnetic field on the order of kilo-Gauss can dampen the buoyancy-induced convection. The computed effective segregation coefficient approaches to 1 when the magnetic field exceeds 3 kilo-Gauss, suggesting the achievement of the near-diffusion-controlled growth. Cröll et al. reported that a complete suppression of dopant striations caused by time-dependent Marangoni convection has been achieved with fields of several Tesla [44]. Baumgartl et al. and Ma et al. investigated the effects of static magnetic field in suppressing the g-jitter and acceleration sparks induced convections under microgravity by numerical modellings [45, 46].

Herrmann et al. have employed static magnetic field to suppress the Marangoni convection in the GaAs growth by floating zone method, and striations are still clearly visible in the crystals due to the limited magnetic field strength [46]. It revealed that the applying of a rotating magnetic field may help addressing this issue [47]. Unlike static magnetic field, rotating magnetic field induces an electromagnetically driven flow to counteract the existing one in the melt. The merit of rotating magnetic field is that the field strength can be considerably decreased as compared with the static field case, and therefore it is more technically and financially acceptable. Ge:Ga crystals were grown via the Bridgman method under a rotating magnetic field on Foton-M3,

and a considerably weakened striation pattern as compared to the crystal without applying the magnetic field [48]. Feonychev et al. pointed out that for the floating zone method, the use of rotating magnetic field can result in a reduction of azimuth velocity which is responsible for the striations in the crystals under a proper frequency and field intensity [49]. Dold and coworkers found that by applying a rotating magnetic field to the Bridgman growth of Ga-doped Ge, the impurity striations are decreased in intensity and increased in frequency [50]. However, Feonychev et al. showed that, for the Bridgman method, the rotating magnetic field cannot reduce the segregation or even worse, cause side effects during the crystal growth [49].

On the other hand, Lan et al. performed three-dimensional simulations to investigate the possibility of using ampoule rotation to control segregation and suppress the g-jitter effects during the Bridgman growth [51]. They have shown that under terrestrial conditions, the idea works only when the rotation speed is on the order of 100 rounds per minutes (RPM) [52, 53]. Their work revealed that under microgravity, the rotation speed can be lowered to less than 20 RPM [51]. The modellings reveal that the unsteady nature of the g-jitter is greatly suppressed by rotation and more axisymmetric flow and dopant fields can be obtained. The results demonstrate that the axial segregation is close to the diffusion-controlled limit if the growth distance is much longer than the diffusion length, and the radial segregation is also significantly improved. Moreover, the authors also considered the effect of eccentric rotation and revealed that considerable improvement in the composition homogeneity can still be achieved once the rotation axis does not deviate much from the growth axis.

Besides the uses of external forces, the convective flow can also be modulated through careful designs of the growth apparatus and ampoule. In general, the buoyancy-driven convection level in the melt is determined by the dimensionless Rayleigh number *Ra* [54]

$$\mathrm{Ra} = g\beta\Delta T L^3 \big/ \alpha\gamma \tag{3}$$

where g is the gravitational acceleration, β is the thermal expansion coefficient, ΔT is the destabilizing temperature difference, L is the melt height, α is the thermal diffusivity, and γ is the kinematic viscosity. Besides reducing g, the regulation of the parameters ΔT and L is also a powerful way to ameliorate the convection flow. For instance, the buoyancy-driven convection level can be reduced by a factor 10^3 when L decreases from 10 to 1 cm. On the other hand, reducing ΔT is also an effective way to suppress the buoyancy-driven convection.

In the common Bridgman furnace design, the heat is supplied radially inward which causes a radial temperature gradient. This design results in a concave growth interface and convective mixing in the melt and, therefore, gives rise to a notable macroscopic segregation. The numerical simulation performed by Ostrogorsky reveals that this effect can be ameliorated by supplying the heat axially instead of radially by using a submerged heater coupled with a guarding heater surrounding the enclosed melt [55]. The typical curve of temperature versus radial position in the melt and crystal regions shows that a significantly reduced radial temperature gradient is

achieved. Ostrogorsky also shows that by using a guarding heating source around the enclosed melt, both the macroscopic and microscopic homogeneity of the crystals are greatly improved. Moreover, the insertion of the submerged heater greatly reduces the parameter L, which can also contribute to the alleviation of convection. Using this method, uniform doping of Te in InSb has been realized on the earth in both the axial and radial directions, suggesting the occurrence of near-diffusion-controlled growth [56]. Replacing the submerged powered heater by an unpowered plate-like baffle, a uniform, steady-state Te segregation was still observed in Te-doped GaSb crystals [57]. According to analytical model and scaling analysis, this scheme applies to the system with equilibrium distribution coefficient in range from 0.3 to 1.0 and low diffusion coefficient [58]. Recently, Te- and Zn-doped InSb crystals were grown under microgravity by using the submerged baffle structure at the International Space Station [54, 59, 60].

3 Detached Solidification

3.1 Observations and Merits of Detached Solidification

In ground-based vertical Bridgman solidification, the outer-surface of the resulting crystal replicates the inner-surface of the crucible. By comparison, directional solidification under microgravity usually results in the so-called detached growth [5]. During detached growth the melt contacts with the crucible wall whereas the crystal grows without touching the crucible, as schematically shown in Fig. 3 [61]. As a result, a narrow gap, typically on the order of 10^{-5} m, appears between the crystal and the crucible wall where a vapor resides. The melt above the gap is supported by the formation of a liquid meniscus between the out edge of the growing crystal and the container wall. Detached growth was firstly observed in the Te-doped InSb crystal grown in Skylab by Witt et al., in which the diameter of the crystal was a little smaller than that of the container [8, 62]. Similar results were found in the subsequent microgravity experiments performed on various semiconductor materials, including Ge, GaSb, GaInSb, InAs, CdTe, CdZnTe, HgCdTe, and so on [63]. In these experiments, a wide spectrum of detached configurations including bubble, necking, shrinkage and wavy surface were observed. A comprehensive review of these observations has been conducted by Cröll et al., and Regel et al., in references [62, 64].

During the ground-based normal Bridgeman growth, the crystal adheres to the crucible wall which leads to considerable thermal mismatch due to the difference in the thermal expansion coefficients of the crystal and the crucible material. For instance, the thermal expansion coefficient of quartz is $\sim 5\times10^{-7}$/K, an order of magnitude lower than those of the commonly used semiconductors. Such a thermal mismatch results in an increased defect (such as dislocation) density or even worse, macroscopic cracks in the grown crystals. As a sharp contract, the lack of direct

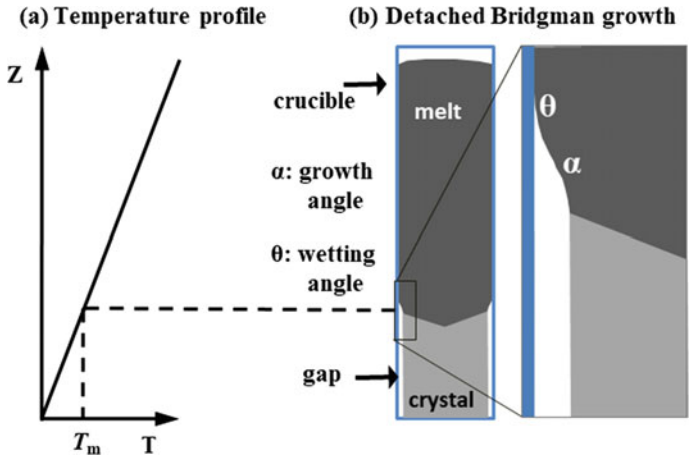

Fig. 3 **a** Temperature profile together with **b** the schematic illustration of the detached Bridgman growth configuration

contact between the grown crystal and the container crucible in the detached growth provides an effective way to reduce the defect density and therefor to improve the total crystal quality [61]. Experiments demonstrated it is true that detached growth can result in a decline of the etched (dislocation) pit density (EPD) and an improved crystallographic perfection. For example, Dold et al. and Schweizer et al. found that Ge crystals grown by detached growth exhibit an EPD reduction of ~2 orders of magnitudes [65, 66]. Similar results were also observed for CdZnTe crystals prepared under μg condition in the detached part [67]. The most striking report is that the EPD of the space InSb crystal can be reduced to $2.5 \times 10^1/cm^2$, far lower than that (10^4 to $10^5/cm^2$) prepared under terrestrial conditions [63]. The greatly reduced EPD has important implications for the device applications of the crystals. For example, GaAs wafers obtained from the earth and space were used to fabricate analogy switch integrated circuits, and the tests revealed that the threshold voltage of backgating, the photosensivity, and the average turn-on time for the space-grown samples are all superior to those of the terrestrial counterparts [2].

Here we stress that although detached growth seems to be a typical feature of the flight experiments, the microgravity condition itself is not necessarily associated with detached growth of semiconductors. It was found that the grown materials, the growth processes, the designed ampoule structures, and the chosen crucible materials, all together determine a growth detached or attached. Despite the consensus that hydrostatic pressure plays an important role in the detachment, the underlying origins of detached growth were not fully understood in a rather long period of time. Moreover, it is highly desirable to reproduce detached experiments on the earth due to the on-going demands on high-quality semiconductor crystals. On the other hand, it is noteworthy that although detached growth was frequently observed, the obtained crystals are not uniform in diameters. Elucidating the underlying

mechanism of detached growth helps providing a possible way towards controllable growth of semiconductor crystals with uniform diameters on the earth, which may open up a new way for cost-effective practical applications.

3.2 The Underlying Mechanism

It was shown geometrically that detachment would occur if $\theta + \alpha \geq 180^{\circ}$, provided that no pressure appears [61]. The two angles, θ and α, denote to the wetting angle of the melt on the crucible wall and the growth angle, respectively (Fig. 3). Generally, the growth angle α mainly depends on the chosen materials and the crystal orientation. For most of the semiconductors, the growth angle ranges from 10° to 30°. Therefore, to achieve detached growth the wetting angle should be 150–170° or even larger, which provides a strict constraint on the selection of crucible materials. Deviations to the $\theta + \alpha \geq 180^{\circ}$ criterion also appeared in literature. For instance, Wang et al. observed detached growth in the InSb system in which the sum of growth angle and wetting angle is far less than 180° [68]. Their results show that besides the material properties, detached solidification also depends on the operating parameters. The reduced value of $\theta + \alpha$ can be ascribed to the introduction of a flux of gas into the gap through the meniscus, which leads to an increase of the pressure in the bottom gas reservoir.

The introduction of additional pressures in the system makes it more complex to derive the conditions needed for the detached growth. The hydrostatic pressure of melt and the vapor pressure difference in the volumes below and above the melt have strong influences on the crystal growth process. Figure 4 schematically illustrates the key factors that influence the contact-free growth. According to the differential Yang-Laplace equation, the pressure difference ΔP across the meniscus is [68, 69]

$$\Delta P = \sigma(1/R_1 + 1/R_2) \tag{4}$$

where σ is the melt surface tension and R_1 and R_2 are the main radii of the curvature (R_1 in the plane of the figure whereas R_2 in the plane perpendicular to R_1), respectively. From Fig. 4, it follows

$$R_1 = -\mathrm{d}s/\mathrm{d}\beta \tag{5}$$

$$R_2 = \mathrm{r}/\cos\beta \tag{6}$$

where s is the curvilinear length along the meniscus, and r is the radial coordinate. The pressure difference across the meniscus can be expressed as

$$\Delta P = \Delta P_o + z\rho \boldsymbol{g} \tag{7}$$

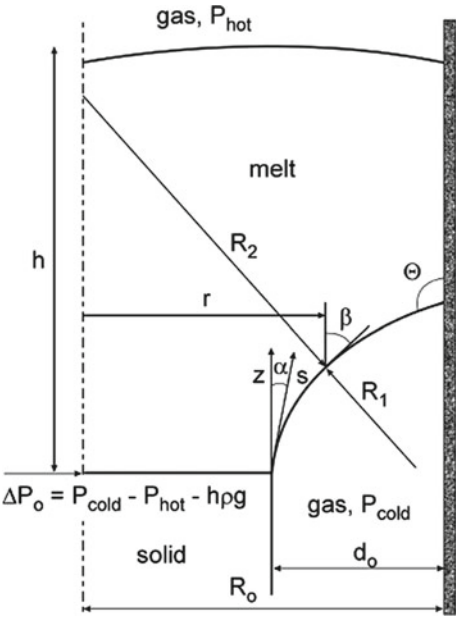

Fig. 4 Schematic diagram of the meniscus region during the detached growth. P_{cold} and P_{hot} are gas pressures below and above the melt, h is the height of the melt, R_0 the radius of the crucible, and R_1 and R_2 are the meniscus radii (R_1 in the plane of the figure, R_2 in the plane perpendicular to R_1). Reprinted with permission from reference [68]

where $\Delta P_o(P_{cold} - P_{hot} - h\rho \boldsymbol{g})$ is the pressure difference at the three phase junction, ρ the melt density, and $\boldsymbol{g}$ the gravitational acceleration. From Eq. (7) it is clear that the pressure difference is determined by the vapor pressure above the melt (P_{hot}), the vapor pressure below the melt (P_{cold}), and the hydrostatic pressure. Based on Eqs. (4)–(7), it can de deduced that

$$\mathrm{d}\beta/\mathrm{d}s - \cos\beta/r = -(P_{cold} - P_{hot})/\sigma + \rho \boldsymbol{g}(h - z)/\sigma \tag{8}$$

A very important implication of Eq. (8) is that the meniscus shape is dependent on the vapor pressures below and above the melt, the hydrostatic pressure, and the melt surface tension. Equation (8) indicates that if the pressure difference varies linearly with the solidification length, the solidification itself does not affect the meniscus shape, i.e., it can be treated as steady-state problem. Under boundary conditions that $\beta = 180^{\circ} - \theta$ at the crucible wall and $\beta = \alpha$ at the gap distance of d_0, the meniscus shape can be computed numerically [68, 69]. It is noted that a growth parallel to the crucible wall is anticipated at a gap width of d_0, given that $\beta = \alpha$ at the three phase line. Any deviation of β from α would result in the crystal growth towards or away from the crucible wall, i.e., the change of the gap width.

In general, the numerical solutions can be divided into two categories: $\theta + \alpha < 180^\circ$ and $\theta + \alpha > 180^\circ$ [61, 68, 69]. Figure 5 shows the dependence of gap width on the pressure difference across the meniscus for $\theta + \alpha < 180^\circ$. The calculation was based on Ge, and the growth angle, surface tension and the inner crucible diameter was selected as 11°, 0.5969 N/m and 12 mm, respectively [68]. It can be seen that to achieve a growth parallel to the crucible wall, a small negative or positive pressure difference is needed. The maximum gap width, on the order of several hundred microns, occurs at $\Delta P_m \approx -2$ mbar. According to the Lyapunov stability criterion, the gap width is stable if $\partial\beta/\partial r < 0$, i.e., the meniscus curvature at the crystal/melt interface is convex [68]. When the meniscus at the crystal/melt interface is concave with respect to the melt, the growth is dynamically unstable. For the concave meniscus case, any perturbation of the meniscus would lead to a sudden change of the growth direction. If the solidification direction is swung to the crucible wall, stable attached growth occurs. Calculations show that $\partial\beta/\partial r < 0$ is tenable when ΔP_m is less than -1 mbar. However, the gap width drops drastically to the value that is comparable with the roughness of the crucible wall, as ΔP_m decreases from -2 mbar. Under this situation, the gap tends to disappear and the complete detachment is not available. Considering these facts, the stable detached growth is possible only in the ΔP_m range of -2 mbar $< \Delta P_m < -1$ mbar. Figure 6 shows the gap width as a function of pressure difference for the $\theta + \alpha > 180^\circ$ case [69]. Under negative pressure difference, the calculations reveal that the meniscus is convex with respect to the melt. That is, a stable gap width can be maintained in a rather broad ΔP_m range of $\Delta P_m < 0$ mbar. However, for ΔP_m very close to 0 mbar, the gap width is so large that the melt run-down occurs under terrestrial conditions. Moreover, for very high pressure difference, $\Delta P_m < -30$ mbar, the gap width is too small to guarantee a true detached solidification.

Figures 5 and 6 also reveal that, the larger the sum of θ and α, the easier the realization of the contact-free growth. Since the wetting angle of Ge on BN is much larger than that on fused silica, the use of BN crucible is beneficial for the realization of detached solidification of Ge. On the other hand, the growth angle of InSb (20–30°) is higher than that of Ge (7–13°), and therefore detachment is more frequently observed during the Bridgman growth of InSb. To achieve detached growth for a given semiconductor material, the chosen crucible should have a wetting angle as large as possible with the semiconductor melt. The contact angles of various semiconductor melts on the commonly used crucible materials are listed in Table 1. Because the surface condition has a close correlation with the wetting angle, any surface contamination should be eliminated before the ampoule preparation. Moreover, since rough surface favors for an increased wetting angle, utilization of crucibles with coarse side surface is beneficial for detached growth. However, rough crucible walls usually enhance heterogeneous nucleation and therefore may cause polycrystalline growth.

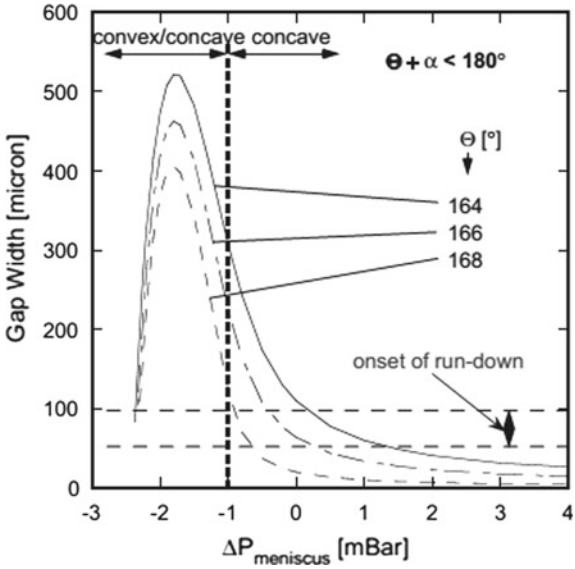

Fig. 5 Gap width as a function of pressure differential across the meniscus for $\theta + \alpha < 180°$. Reprinted with permission from reference [69]

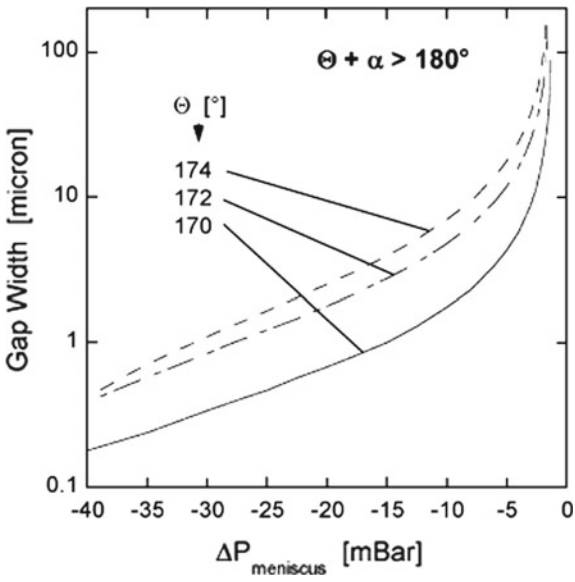

Fig. 6 Gap width as a function of pressure differential across the meniscus for $\theta + \alpha > 180°$. Reprinted with permission from reference [69]

Table 1 Contact angles of various semiconductors on commonly used crucibles

Crucibles	Semicond.				
	Si	Ge	InSb	GaSb	CdTe
Fuzed silica	87 [70]	117 [71]	165–175 [72]	130 [73]	83–108 [74]
BN	145 [75]	173 [71]	134 [76]	132 [77]	132 [74]
Graphite	10–30 [78]	166 [71]	124 [76]	129 [77]	

3.3 Guides to Ground-Based Solidifications

As discussed in Sect. 2, the pressure difference across the meniscus has two sources—the pressure difference between vapors in the gap and above the melt, and the hydrostatic pressure. Provided that the density of the semiconductor melt is 5 g/cm^3 and the melt height is 10 cm, the hydrostatic contribution to the pressure difference across the meniscus under 1-g_0 condition is -50 mbar. Such a value is one order of magnitude larger than what is needed by the detached solidification, under both $\theta + \alpha < 180^\circ$ and $\theta + \alpha > 180^\circ$. This explains why detachment has scarcely been observed in the Bridgman growth on the earth. To meet the criterions for detachment illustrated in Sect. 2, an overpressure in the gap is of vital importance for the solidification processes performed on the earth.

There are various methods to generate the overpressure in the gap: (i) active control of the pressure difference by using an external gas source, (ii) inducing overpressure via temperature gradient variation, and (iii) the creation of overpressure by introducing internal gas source. The latter one is applicable for the compounds in which one element has a higher saturated vapor pressure than the others, and has been successfully utilized to the CdTe system [79]. The drawback of this method is that the adding of volatile element into the ampoule can induce the non-stoichiometry of the grown crystals.

The former two methods are not restricted to the volatile compounds like CdTe, but also apply to other material systems. Duffar et al. have proposed the active pressure control scheme and used it to grow InSb crystals [69, 80]. They designed an ampoule architecture in which the top part and the bottom part are connected to the gas systems through openings, and therefore the pressures in these two parts can be controlled separately. Using this method the overpressure in the bottom part can be easily tuned to close to the hydrostatic pressure of the melt and, as a result, contact-free growth was achieved over the entire length of the sample under 1-g_0 condition. As the growth proceeds, the gap in the bottom part of the ampoule increases in volume and thus the static pressure decreases. To insure stable detached solidification and control the crystal radius, the vapor pressure has to be tuned continuously to compensate this gap increase. Yeckel et al. scheduled a scheme to incorporate the proportional-integral (PI) feedback controller to stabilize the detached vertical Bridgman growth [81]. This is very challengeable due to the fact that detached growth is a strong nonlinear process. Very recently, they also investigated the possibility to manipulate the gas

pressure through nonlinear feedback control [82, 83]. Their results show that both the solution multiplicity and the strict operability limits encountered by using the linear PI controller are well addressed.

Another efficient way to achieve detached growth is inducing an axial temperature gradient variation, as proposed by Szofran et al. [84]. In this approach, the sealed crucible is filled with inert gas and then the feed material is molten using the normal Bridgman temperature profile. The melting of the feed material isolates the two gas reservoirs located at the top and bottom of the crucible. After that, the temperature in the top crucible region is lowered which results in a notable vapor pressure difference. Owing to the overpressure in the bottom reservoir, a meniscus is formed and the crystal starts to grow without contact to the crucible. To achieve the desired axial temperature gradient change, a furnace with multiple heating zones and separate temperature controls is needed. As the growth proceeds, the crystal moves out of the modified temperature profile, resulting in the breakdown of detached growth. To address this issue, the temperature in the top crucible region should be tuned successively during the growth. Duffar et al. [85] modified this method by introducing a gas reservoir below the seed and separately controlling its temperature through an additional heating zone. The experimental results revealed that this improved approach is self-controlling in terms of pressure adjustment [85].

Experimental results demonstrate that the detached growth is highly beneficial for improving the quality of ground-based crystals. Figure 7 presents the surface images of detached and attached Ge crystals grown on the earth [65]. For the detached growth of Ge, the typical gap width is ~10 μm. The samples were etched for 10 min at 85 °C with the Billig etchant which is prepared by dissolving 12 g KOH and 8 g $K_3[Fe(CN)_6]$ into 100 ml H_2O. As can be clearly seen in Fig. 7, detached growth leads to an EPD reduction as high as two orders of magnitude in the edge regions of the crystals. It is known that the EPD of the ground-grown crystals via vertical Bridgman

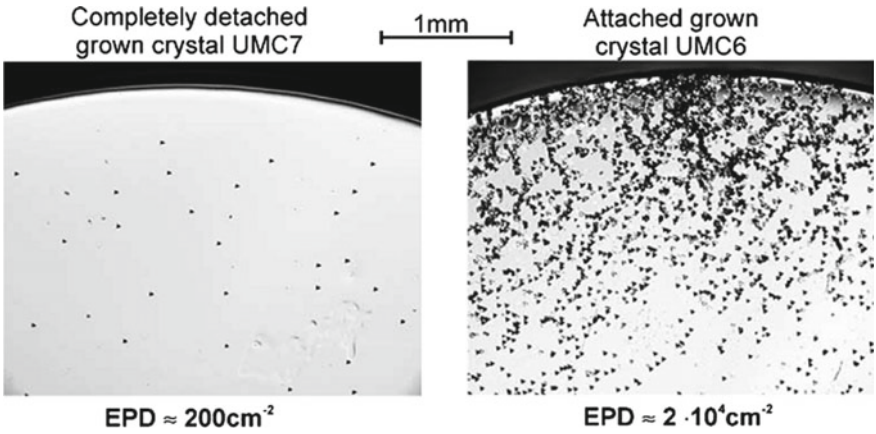

Fig. 7 Surface photographs of the detached and attached Ge crystals. Reprinted with permission from reference [65]

method is on the orders of 10^3 to $10^8/cm^2$. The edge region of the detached Ge crystal has an EPD as low as $2 \times 10^2/cm^2$. In the middle of the crystals, detached growth also results in a notable reduction of EPD from $7 \times 10^3/cm^2$ to $5 \times 10^2/cm^2$. The results are further confirmed by X-ray topography using synchrotron radiation which show that the EPD decreases from $10^4/cm^2$ in the seed to 10^2 to $10^3/cm^2$ in the detached crystal. Similar observations were also observed in other semiconductor materials. Obviously, the understanding of the mechanism of detached growth and the guide to terrestrial experiments are one of the greatest achievements in the microgravity materials research.

3.4 Implications of Detached Growth Mechanism for Microgravity Experiments

As discussed in Sect. 3.2, semiconductor melts are fluids with low Prandtl number, which are characterized by high thermal conductivity and low viscosity. Due to this fact, stabilized natural convection cannot be observed in semiconductor melts on the earth. However, it is hard to fully understand and account for the natural convection featured with unsteady and random flow patterns using the analytical tools. Under microgravity conditions, the natural buoyancy-driven convection is greatly reduced which makes it possible to realize the diffusion-controlled segregation. The diffusion-controlled segregation simplifies the growth process and the growth parameters such as diffusion coefficient can be derived analytically. However, due to the residual acceleration and the appearance of free surface, true diffusion-limited process is not available in most cases. We have shown in Sect. 3.2 that the influence of residual acceleration can be dampened by applying a magnetic field or using a submerged baffle. On the other hand, free surfaces are frequently observed in semiconductor melts due to detached growth during the flight experiments. The in-depth understanding of detached growth provides powerful measures to eliminate free surfaces.

Ostrogorsky et al. have performed series of Bridgman solidification experiments on Te-doped InSb in the Microgravity Science Glovebox (MSG) at the International Space Station (ISS) [60]. To preclude the influence of Marangoni convection, all the charges were pressurized by specially designed piston and spring devices to prevent the occurrence of de-wetting. The furnace in MSG is equipped with a viewing port, and the growth interface can be visualized via the in situ observation system. Real-time observations revealed that de-wetting did not occur on the side of the crystal. The dopant distribution was measured by secondary ion mass spectrometry, and a typical result along the central axis of the crystal is shown in Fig. 8. A diffusion coefficient of 1×10^{-5} cm^2/s, several times lower than previously reported values, provides a reasonably good fit to the data using the one-dimensional diffusion-controlled segregation relationship. Reproducible initial transients in dopant concentration were observed in other Te-doped InSb growths in the series of experiments.

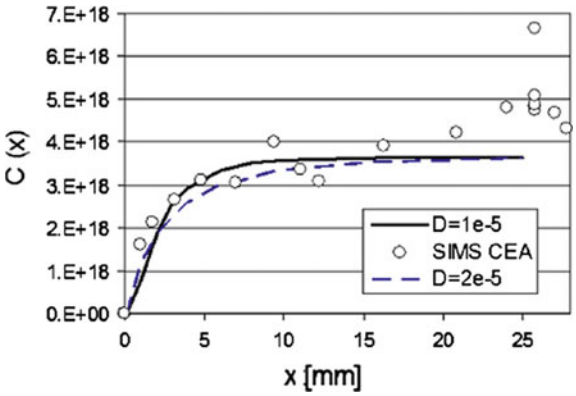

Fig. 8 Dopant segregation profile of the Te-doped InSb crystal grown at ISS; the solid and dashed lines are based on finite element calculations using diffusion coefficients of 1×10^{-5} cm^2/s and 2×10^{-5} cm^2/s, respectively. Reprinted with permission from reference [59]

Zn-doped InSb solidifications were also performed at ISS using the similar ampoule configuration [61]. To prevent the formation of free surfaces, a static pressure of ~40 mbar was applied on the melt through a piston controlled by the carbon spring. A diffusion-controlled initial transient was also observed, with a fitted Zn diffusion coefficient of 1.2×10^{-4} cm^2/s. Zn-doped InSb has an equilibrium distribution coefficient of 2.9 and materials systems with $k > 1$ were scarcely studied in the microgravity experiments. The work performed on Zn-doped InSb is the first one that reports diffusion-controlled growth for systems with $k > 1$. All these results show that by damping the formation of free surface based on the knowledge of detached growth, new experimental schemes were designed and an in-depth understanding of the microgravity solidification process has been achieved.

4 New Melt Growth Techniques

4.1 Difficulties in Preparing Semiconductor Alloys

Semiconductor alloys (or concentrated semiconductors), such as $Ge_{1-x}Si_x$, $In_xGa_{1-x}Sb$ and $In_xGa_{1-x}As$, are of considerable interest for technological applications since their physical properties, including lattice constants, electronic performance and optical bandgaps can be tuned simply by controlling the alloy composition. For example, $In_xGa_{1-x}Sb$ is an important opto-electric material which exhibits an enhanced thermoelectric performance than InSb due to its proper bandgap [85]. On the other hand, it is well known that $Ge_{1-x}Si_x$ is very promising for seamlessly connecting the optoelectronics and microelectronics on the Si-based platforms [86]. Due to these facts, there has been attracted considerable interest

in semiconductor alloys in recent years. However, it is difficult to grow large-size, chemically homogeneous Semiconductor alloy crystals because the large separation between the solidus and liquidus lines in the pseudo-binary phase diagrams. The attempts to grow semiconductor alloys via traditional techniques, e.g., Bridgman method, fail to produce homogeneous crystals, even under microgravity conditions [22, 23]. The obtained crystals have compositions vary considerably along the axial and radial directions, and cannot meet the needs for actual applications.

Under the diffusion-controlled steady-state growth, there occurs a boundary layer adjacent to the growth interface where a solute concentration gradient (solute concentration varies from C_0/k to C_0) is built. Any perturbation near the boundary would break the delicate balance and produce a variation of the solute concentration gradient and therefore, leading to a notable segregation in the crystal. This effect is particularly strong for a system which has a large separation between the solidus and liquidus lines in the pseudo-binary phase diagrams near the targeted composition. To address this issue, researchers proposed new schemes which yield more stable solute profiles in the melt. These new schemes are the traveling liquidus-zone (TLZ) method and the vertical gradient freezing (VGF) method. The key of these methods relies in the degree of saturation in the melt—the melt is saturated and therefore the solute concentration is equivalent to that on the liquidus line. This feature distinguishes these two methods from other techniques. On condition that the slope of liquidus line is a constant, the solute concentration gradient in the melt is proportional to the temperature gradient. Based on these two methods, chemically homogeneous $Ge_{1-x}Si_x$ and $In_xGa_{1-x}Sb$ single crystals were grown under microgravity.

4.2 TLZ Method and Related Microgravity Experiments

The TLZ method is a zone-melting method proposed and developed by Kinoshita et al. [89] As discussed in Sect. 4.1, the most important feature of TLZ is that it has a saturated liquidus-zone. The study on this method starts from $In_xGa_{1-x}As$, and latterly applies to the $Ge_{1-x}Si_x$ system [89].

Figure 9 schematically shows the principle of the TLZ method (taking the InAs-GaAs system as an example). According to the InAs-GaAs phase diagram, the InGaAs ($In_{0.3}Ga_{0.7}As$) crystal growth needs a freezing interface temperature of ~1027 °C, a linear temperature gradient of ~15 °C/cm, and a zone width of ~20 mm. In this case, the solute concentration gradient can be controlled by the imposed temperature gradient because the solute concentration is determined by the temperature on the liquidus-line

$$\left(\frac{\partial C_L}{\partial Z}\right)_{Z=0} = \left(\frac{\partial C_L}{\partial T}\right)_{Z=0}\left(\frac{\partial T}{\partial Z}\right)_{Z=0} \tag{9}$$

where C_L is the solute concentration at the liquidus line, T is the temperature, Z is the distance measured from the freezing interface, and $\frac{\partial T}{\partial Z}$ is the temperature gradient.

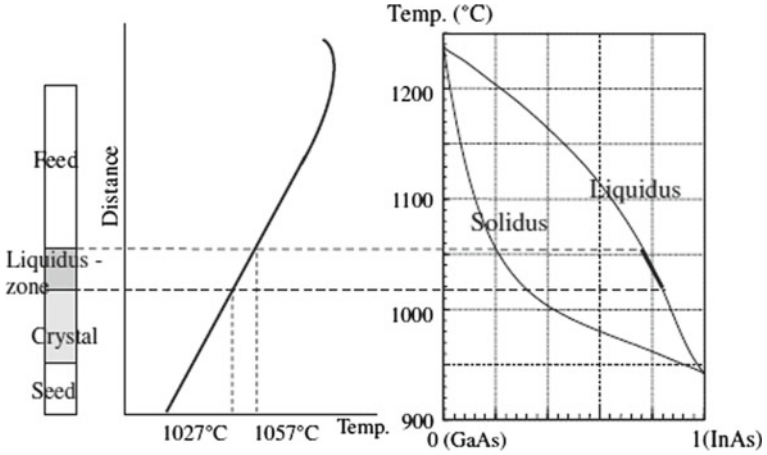

Fig. 9 Sample configuration and the corresponding temperature profile of the TLZ method for the InAs-GaAs system. Reprinted with permission from reference [87]

Therefore, $\frac{\partial C_L}{\partial T}$ represents a reciprocal of the slope of the liquidus-line at around the interface temperature. Furthermore, the freezing rate, R, can be written as

$$-R(C_{Lo} - C_{so}) = D(\partial C_L/\partial Z)_Z = 0 \tag{10}$$

where C_{L0} and C_{S0} are the liquidus and solidus solute concentrations at the freezing interface, and D is the inter diffusion coefficient between solute and solvent. According to the Eq. (10), the freezing rate can be expressed as

$$-R = -\frac{D}{(C_{l0} - C_{s0})}\left(\frac{\partial C_L}{\partial Z}\right)_{Z=0} = -\frac{D}{(C_{l0} - C_{s0})}\left(\frac{\partial C_L}{\partial T}\right)\left(\frac{\partial T}{\partial Z}\right)_{z=0} \tag{11}$$

A very important point obtained from Eq. (11) is that the freezing rate is determined by the temperature gradient ($\partial T/\partial Z$). As a result, it is easy to maintain the freezing interface temperature at a constant value by translating the sample at a speed of R. The relationship between $R$and ($\partial T/\partial Z$) in Eq. (11) is determined by measuring the growth rate R and the temperature gradient near the interface, and by comparing the measured growth rate with the calculated one. Kinoshita et al. have successfully grown homogeneous InGaAs and SiGe single crystals using the TLZ method on ground, and the chemical inhomogeneity is lower than 1% within the whole growth areas, both along the axial and radial directions [88–90].

Although the TLZ method has been used for growing semiconductor alloys on ground [88, 89], it is still a great challenge to fabricate large-diameter crystals with homogeneously distributed chemical compositions on the earth due to the influence of buoyancy-driven convection. To address this issue, microgravity crystal growth experiments performed by the TLZ method are highly desirable. Kinoshita et al.

reported the growth of SiGe alloy crystal with a diameter of 10 mm in and a growth length of 17.2 mm by the TLZ method under microgravity [91]. The concentration of Ge is about 48.5 ± 1.5 at % along the center line of the grown crystal, and the peripheral concentration profile reveals a similar Ge concentration. That is, both the axial and radial concentration variations are small [92, 93]. They also found that the growth length was short for the crystal grown at higher temperature gradient, due to the strong influence of constitutional supercooling. Numerical simulations of the SiGe crystal growth via the TLZ method were also carried out by the same gr.

4.3 The VGF Method

Conventional methods such as Czochralski and Bridgman techniques are difficult to grow $In_xGa_{1-x}Sb$ single crystals with enough size and high quality due to the buoyancy-driven convection on ground. Therefore, many scientists have done their best to overcome this problem through various methods. Tsuruta et al. developed the ultrasonic-vibrations-introduced Czochralski method to reduce the degree of supercooling. When the $In_xGa_{1-x}Sb$ mixed crystal is grown by introducing ultrasonic vibrations into the melt, the facet growth appear firstly, and the facet growth regions has a high concentration of in matrix component and Te impurity compared to the normal growth region [94–96]. Czochralski method with multi-step pulling was applied to Ga-In-Sb ternary solution for growing GaInSb bulk crystals [97]. Dutta et al. demonstrated that forced convection or mixing in the melt during directional solidification of bulk $In_xGa_{1-x}Sb$ ternary alloys significantly decreases cracks in the crystals [98]. Floating crucible Czochralski method was used to prepare InGaSb polycrystalline crystals, and the results show that although axial segregation can be ameliorated, the reproducibility is still a challenge [99]. As for GaInSb alloys prepared by Bridgman method, the growth at a variable pulling rate can improve the axial chemical homogeneity [100]. Numerical simulations certified that an alternating magnetic field applied near the solid-liquid interface increases the melt flow intensity, and has a notable effect on the radial segregation and the interface deflection [101, 102]. Although considerable efforts have been devoted to the InGaSb growth, it is still a great challenge to achieve chemical homogeneity in this system.

The VGF method is very promising for addressing this issue. The VGF method is different from TLZ in that the sample does not shift during the whole growth process. Instead, homogeneous semiconductor alloys can be grown using VGF by cooling the sample at a fixed cooling rate, on condition that the liquidus temperature at the growth interface keeps constant (Fig. 10). Figure 10a, b show the ampoule configuration and the temperature profile of the furnace. The feed and the seed were placed at the high and low temperature regions, respectively. The sample is composed of three parts: the seed, the low temperature zone and the feed, as shown in Fig. 10c, d. Before growth, the system is heated to a temperature that turns the low temperature material into molten melt. Parts of the seed and feed are dissolved into the liquid zone and thus a solution forms. After that, the crystal growth begins by slowly decreasing the

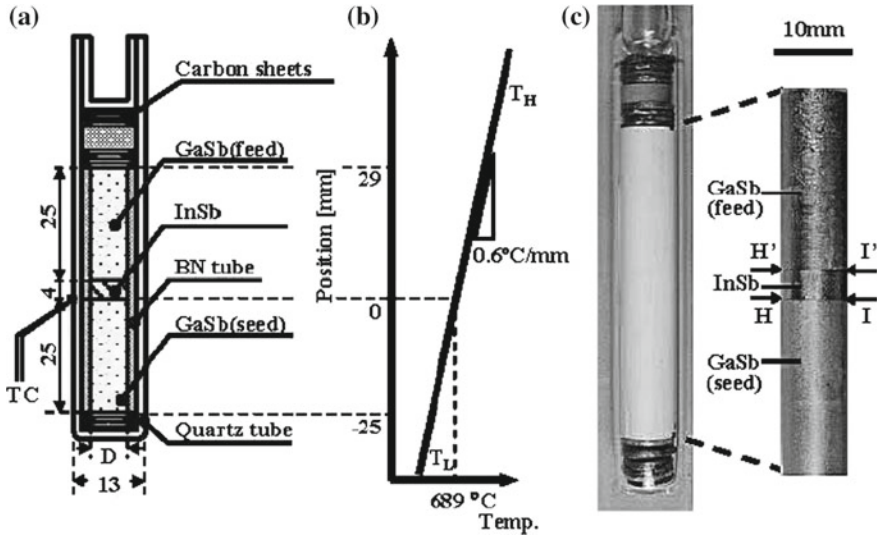

Fig. 10 The vertical gradient freezing method (taking the growth of InGaSb as an example): **a** Ampoule configuration, **b** the temperature profile in the furnace, **c** the ampoule before growth, and **d** the sample before growth. Reprinted with permission from reference [103]

furnace temperature. During the growth, the solid-liquid interface moves towards feed. As a result, homogeneous alloy crystals can be grown by the VGF method.

We now take the growth of $In_{0.03}Ga_{0.97}Sb$ as an example (Fig. 11). The ampoule which locates in the furnace is heated slowly up to the growth temperature T_H, and then the furnace is kept at this temperature for 20 h. During the holding time, InSb melts at its melting point 525 °C and GaSb seed and feed crystals dissolve in the InSb melt to form InGaSb solution. The temperature gradient is kept at 0.6 °C/mm, and the temperature of the feed interface is higher than that of the seed interface. Since the dissolution of GaSb feed is faster than the seed, a compositional gradient between the seed and feed interfaces is formed. When the low temperature seed interface becomes supersaturated, the crystal growth starts and interface moves gradually towards the feed. The key issue for the VGF growth is setting the cooling rate—at a proper cooling rate, the interface moving speed equals to R (Eq. 11) and the liquidus temperature near the growth interface maintains at a constant value. At such a cooling rate, homogeneous semiconductor alloys can be successfully grown. The optimum cooling rate for $In_{0.03}Ga_{0.97}Sb$ growth is 0.15 °C/h, under the temperature gradient of 0.6 °C/mm.

Murakami and coworkers have measured the growth rate using a GaSb(seed)/InSb/GaSb(feed) sandwich sample by characterizing the distances of the Te striations which were intentionally introduced into the grown crystal through thermal pulses [104]. The composition profiles reflect the change of growth rate, which show that the growth rate gradually increases to the saturated value and then rapidly decreases. The same group also explored the possibility of growing $In_xGa_{1-x}Sb$

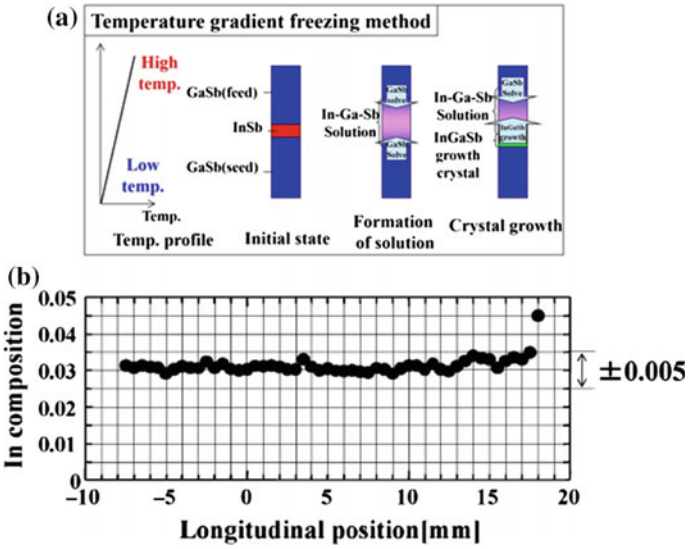

Fig. 11 **a** The schematic of vertical gradient freezing method. **b** Indium composition profile of InGaSb crystal with a cooling rate of 0.15 °C/h. Reprinted with permission from reference [103]

bulk crystals through a InSb seed by using a InSb(seed)/Te-doped InSb/GaSb(feed) sandwich structure [105]. Homogeneous $In_{0.8}Ga_{0.2}Sb$ and $In_{0.6}Ga_{0.4}Sb$ crystals were grown at cooling rates of 0.77 and 0.33 °C/h, corresponding to the growth rates of 0.45 and 0.19 mm/h, respectively. Hayakawa et al. developed an in situ X-ray penetration method to study the composition profiles of the In-Ga-Sb solution [106]. Rajesh et al. observed the detailed dissolution process of GaSb into InSb by using this method with a CdTe detector [107]. The gallium (Ga) composition profile of the sample was successfully calculated as a function of time by making the calibration line with the penetrated X-ray intensities of GaSb and InSb standard samples.

4.4 Microgravity Experiments Based on VGF

The viscosity, wetting property and evaporation rate of InSb, GaSb and $In_xGa_{1-x}Sb$ were studied for the crystal growth experiments at the International Space Station. The results indicate that the viscosity of $In_xGa_{1-x}Sb$ decreases with the increase of Indium, and the determined value is between those of InSb and GaSb. No noticeable wetting reaction between the molten $In_xGa_{1-x}Sb$ and the quartz, BN and graphite substrates was observed, revealing that these substrate materials can be used to fabricate crucibles for the $In_xGa_{1-x}Sb$ microgravity experiments [33]. Based on these results, an optimized ampoule structure was designed and used in the microgravity experiment by Japan Aerospace Exploration Agency. Inatomi et al. have grown the

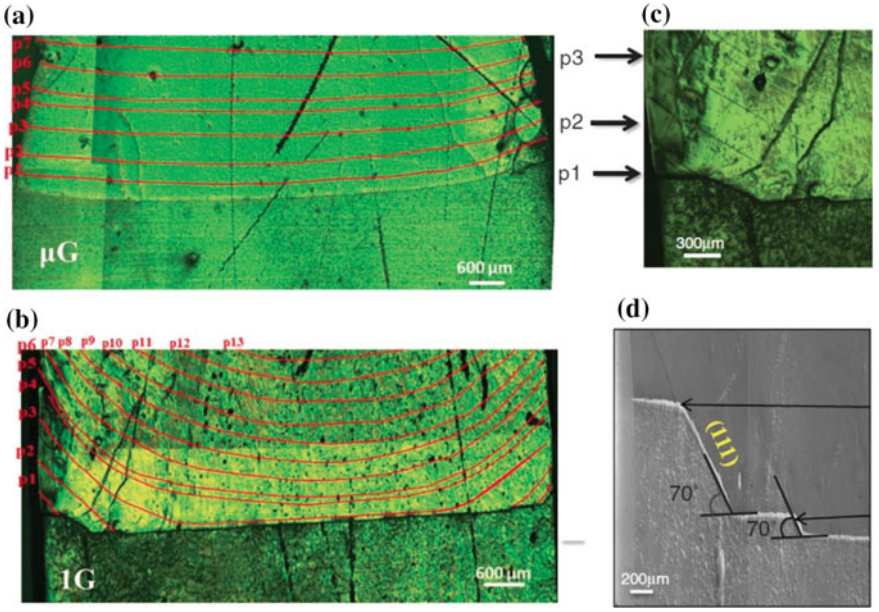

Fig. 12 Polarized optical microscope images of the etched surfaces of **a** μg and **b** 1 g samples. **c** Optical micrograph and **d** field emission scanning electron microscopy image at the periphery of the 1 g sample. The dopant striations are marked as p1, p2 and p3 in (**c**). Reprinted with permission from reference [108]

$In_xGa_{1-x}Sb$ crystals via the VGF method mentioned above under μg conditions at the International Space Station, and the dissolution and growth processes were carefully studied [28]. The optical micrographs of the un-dissolved seed interface in the space- and ground-based samples are shown in Fig. 12. By applying heat pulses, striations were introduced into the crystal and the growth rate was determined. It can be clearly seen in Fig. 12 that the space-based crystal has a rather flat growth interface. By sharp comparison, the crystal grown on earth has a concave growth interface. Moreover, the etch pit density of the μg_0 sample was lower than that of the 1-g_0 samples, indicating the μg_0 crystal has a higher quality. The above results clearly show that the buoyancy-driven convection affects both the crystal quality and the solid-liquid interface shape.

The measurements on the composition profiles of the crystals along the growth direction show that the $In_xGa_{1-x}Sb$ crystal growth under μg_0 starts from 20.2 mm and ends at 35.1 mm; therefore, the growth length was 14.9 mm. By comparison, the 1-g_0 crystal growth starts from 18.0 and ends at 30.6 mm, and the total growth length is 12.6 mm. The amount of indium gradually decreases along the growth direction and fluctuates severely at the regions $x > 35.1$ and > 30.6 mm for the μg_0 and 1-g_0 samples, respectively. The remaining solution rapidly solidifies due to the crystal cooling after the growth period, leading to the observed compositional fluctuations

at the final crystal growth regions. The indium composition of the μg_0 sample at the seed interface was 0.028, much lower than that of the 1-g_0 sample, due to the large amount of seed dissolution on ground. From the InSb–GaSb binary phase diagram, the anticipated growth temperature and temperature gradient can be calculated. However, the obtained temperature gradient for the 1-g_0 growth (0.58 °C/mm) is slightly lower than that of the μg_0 sample (0.64 °C/mm). The crystal growth rate is determined by measuring the grown length between the striations, and the growth rate variations along the growth direction of the μg_0 and 1-g_0 samples are shown in Fig. 12 in reference [108]. The obtained results show that the growth rate of the 1-g_0 crystal is lower than that of the μg_0 sample. Under microgravity, the initial growth rate is about one order of magnitude higher than that under 1-g_0 condition as a result of the absence of buoyancy-induced convection.

InGaSb ternary alloys were also grown by using GaSb $(111)_A$ and $(111)_B$ (Ga-terminated and Sb-terminated faces) seeds and feeds on board the International Space Station by the VGF method [109]. The experiments aim to study the orientation-dependent dissolution and growth of InGaSb along the GaSb$(111)_B$ and $(111)_A$ faces. Assuming the growth of InGaSb crystal in space by VGF is a steady state process dominated by diffusion and the solute was saturated in the solution, the mixed InGaSb crystals growth rate should be directly proportional to the temperature gradient. Therefore, the ratio of growth rates of the $(111)_A$ and $(111)_B$ samples should be same under the same temperature gradients. However, the experimental results show that the $(111)_A$ and $(111)_B$ samples have quite different growth rates (Fig. 13), and the growth rate of the $(111)_B$ face is 15.4% higher than that of $(111)_A$. Apparently, the growth rate is also severely influenced by the concentration gradient $\frac{\partial C_L}{\partial T}$, and the lower growth rate of $(111)_A$ sample has a close correlation with the lower dissolution of the GaSb $(111)_A$ [109]. The growth rates (Fig. 13) at different positions along the growth direction show that the $(111)_A$ face had a lower growth rate than the $(111)_B$ face.

Recently, a Chinese recovery satellite SJ-10 was launched and InGaSb crystals were grown on this scientific platform under gravity level of 10^{-4} to 10^{-5} g_0, by using the VGF method. The grown crystal was cut longitudinally into two pieces along the growth direction and the surfaces were polished by alumina abrasives. The EPMA analysis shows that the high quality $In_{0.11}Ga_{0.89}Sb$ crystal was successfully grown at the Chinese recovery Satellite SJ-10 with a uniform composition distribution.

All these results show that high-quality InGaSb crystals with homogeneous composition distribution can be obtained under microgravity by the VGF method. By sharp comparison, the preparations of InGaSb by other techniques on space did not yield results as good as those obtained by the VGF method [22, 23, 110–112]. Moreover, we note that although the VGF method is mainly used to grow InGaSb, it can also apply to other semiconductor alloy systems.

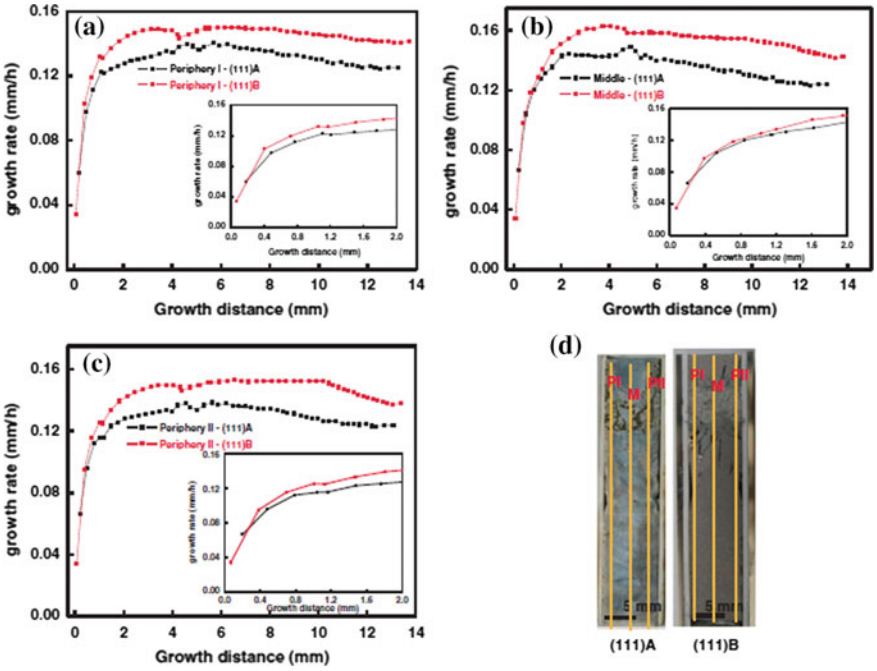

Fig. 13 Growth rates of the InGaSb $(111)_A$ and $(111)_B$ crystals along **a** periphery-I, **b** middle, and **c** periphery-II, **d** crystal surface in which the measured positions are marked by solid lines. Reprinted with permission from reference [109]

5 Conclusion

Melt growth is the most widely used method to fabricate high-quality semiconductor single crystals towards optoelectronic and microelectronic applications. Although the microgravity condition does not always yield the diffusion-controlled growth, the homogeneity of the obtained semiconductor crystals is improved, typically along the axial direction. Based on the microgravity experiments, an in-depth understanding of the interactions among heat transfer, convection, solute transport and chemical segregation, has been achieved. Moreover, with the help of these achievements, active control on the convective flow and the chemical homogeneity is realized via various methods, e.g., by applying a magnetic field during the growth or inserting a submerged baffle in the ampoule.

One of the remarkable breakthroughs in the field of melt growth is the understanding of the detached growth. Detached growth is typically associated with directional solidifications performed on space and is scarcely observed on ground-based experiments. By disclosing the underlying mechanism of detached growth, this magic growth technique can now be realized in the laboratory experiments through improved designs of the ampoules. The most amazing feature of detached growth is

that it can reduce the dislocation density by orders of magnitude, which offers new opportunities for low-cost, high-performance device applications.

There emerge new melt growth techniques, including the traveling liquidus-zone method and the vertical gradient freezing method. These two methods distinguish them from the traditional ones in that they provide a saturated liquid region between the growth interface and the feed material. Under this scheme, a constant composition distribution across the whole growth area is achieved by fixing the temperature at the growth interface. The traveling liquidus-zone method and the vertical gradient freezing method are successfully used to grow chemically homogeneous semiconductor alloys, including $Ge_{1-x}Si_x$ and $In_xGa_{1-x}Sb$, in both the space-based and ground-based experiments. These methods also have great potentials for the growth of other semiconductor alloy systems.

References

1. Benz KW, Dold P (2002) Crystal growth under microgravity: present resultsand future prospects towards the International Space Station. J Cryst Growth 237:1638
2. Chen NF, Zhong XR, Lin LY, Zhang M, Wang YS, Bai XW, Zhao J (2001) Comparison of field effect transistor characteristics between space-grown and earth-grown gallium arsenide single crystal substrates. Appl Phys Lett 78:479
3. Chen NF, Zhong XR, Lin LY, Xie X, Zhang M (2000) Semi-insulating GaAs grown in outer space. Mater Sci Eng B 75:134
4. Kamotani Y, Matsumoto S, Yoda S (2007) Recent developments in oscillatory marangoni convection. EDMP 3:147
5. Ebnalwaled AA, Duffar T, Sylla L (2013) Dewetting and transport property enhancement: antimonide crystals for high performance electronic devices. Cryst Res Technol 48:236
6. Tiller WA, Jackson KA, Rutter JW, Chalmers B (1953) The redistribution of solute atoms during the solidification of metals. Acta Met 1:428
7. Smith VG, Tiller WA, Rutter JW (1955) A mathematical analysis of solute redistribution during solidification. Can J Phys 33:723
8. Witt AF, Gatos HC, Lichtensteiger M, Lavine MC, Herman CJ (1975) Crystal growth and steady-state segregation under zero gravity: InSb. J Electrochem Soc 122:27
9. Zhou YF, Li XY, Bai SQ, Chen LD (2010) Comparison of space- and ground-grown $Bi_2Se_{0.21}Te_{2.79}$ thermoelectric crystals. J Cryst Growth 312:775
10. Witt AF, Gatos HC, Lichtensteiger M, Herman CJ (1978) Crystal growth and segregation under zero gravity: Ge. J Electrochem Soc 125:1832
11. Bly JM, Kaforey ML, Matthiesen DH, Chait A (1997) Interface shape and growth rate analysis of Se/GaAs bulk crystals grown in the NASA crystal growth furnace (CGF). J Cryst Growth 174:220
12. Gillies DC, Lehoczky SL, Szofran FR, Watring DA, Alexander HA, Jerman GA (1997) Effect of residual accelerations during microgravity directional solidification of mercury cadmium telluride on the USMP-2 mission. J Cryst Growth 174:101
13. Strelov VI, Kuranova IP, Zakharov BG, Voloshin AE (2014) Crystallization in space: results and prospects. Crystallogr Rep 59:781
14. Alexander JID, Garandet J-P, Favier J-J, Lizee A (1997) g-Jitter effects on segregation during directional solidification of tin-bismuth in the MEPHISTO furnace facility. J Cryst Growth 178:657
15. Coriell SR, Boisvert RF, Rehm RG, Sekerka RF (1981) Lateral solute segregation during unidirectional solidification and inter-face instabilities during unidirectional solidification of a binary alloy. J Cryst Growth 54:167

16. Griffin PR, Motkef S (1989) Influence of nonsteady gravity on natural convection during microgravity solidification of semiconductors: part I. J Appl Microgravity Technol 2:121
17. Alexander JID, Ouazzani J, Rosenberger F (1989) Analysis of the low gravity tolerance of Bridgman–Stockbarger crystal growth: part I. Steady and impulse accelerations. J Cryst Growth 97:285
18. Naumann RJ (1994) Modeling flows and solute redistribution resulting from small transverse accelerations in Bridgman growth. J Cryst Growth 142:253
19. Derby JJ, Kwon Y, Pandy A, Sonda P, Yeckel A, June T, Müller G (2006) Developing quantitative, multiscale models for microgravity crystal growth. Ann N Y Acad Sci 1077:124
20. Pandy A, Yeckel A, Reed M, Szeles C, Hainke M, Müller G, Derby JJ (2005) Analysis of the growth of cadmium zinc telluride in an electrodynamic gradient freeze furnace via a self-consistent, multi-scale numerical model. J Cryst Growth 276:133
21. Derby JJ, Zhang N, Yeckel A (2013) Modeling insights on the melt growth of cadmium zinc telluride. J Cryst Growth 379:28
22. Duhanian N, Marin C, Abadie J, Chaudet M, Dieguez E, Duffar T (1997) Chemical segregation and crystal crucible interaction during the growth of Ga0.8In0.2Sb in space. Microgravity Sci Technol XI/4:187
23. Duhanian N, Duffar T, Marin C, Dieguez E, Garandet JP, Dantan P, Guiffant G (2005) Experimental study of the solid–liquid interface dynamics andchemical segregation in concentrated semiconductor alloy Bridgman growth. J Cryst Growth 275:422
24. Stelian C, Duffar T (2005) Numerical analysis of solute distribution and interface stabilization during experimental Bridgman growth of concentrated GaInSb alloys. J Cryst Growth 275:422
25. Stelian C, Duffar T (2005) Growth of concentrated GaInSb alloys with improved chemical homogeneity at low and variable pulling rates. J Cryst Growth 275:e585
26. Stelian C, Duffar T (2005) Modeling of a space experiment on Bridgman solidification of concentrated semiconductor alloy. J Cryst Growth 275:175
27. Nakamura S, Hibiya T, Kakimoto K, Imaishi N, Nishizawa S, Hirata A, Mukai K, Yoda S, Morita TS (1997) Temperature fluctuations of the Marangoni flow in a liquid bridge of molten silicon under microgravity on board the TR-IA-4 rocket. J Cryst Growth 186:85
28. Nakamura S, Hibiya T, Kakimoto K, Imaishi N, Yoda S, Nakamura T, Koyama M, Dold P, Benz KW (1999) Observation of periodic Marangoni convection in a molten silicon bridge on board the TR-IA-6 rocket. J Jpn Soc Microgravity Appl 16:99
29. Yano T, Nishino K, Kawamura H, Ueno I, Matsumoto S, Ohnishi M, Sakurai M (2011) Space experiment on the instability of Marangoni convection in large liquid bridge—MEIS-4: effect of Prandtl number. J Phys Conf Ser 327:012209
30. Duffar T, Serrano MD, Lerin L, Santailler JL (1999) Marangoni convective effect during crystal growth in space. Cryst Res Technol 34:457
31. Müller G, Neumann G, Matz H (1987) A two-Rayleigh-number model of buoyancy-driven convection in vertical melt growth configurations. J Cryst Growth 84:36
32. Schweizer M, Cröll A, Dold P, Kaiser T, Lichtensteiger M, Benz KW (1999) Measurement of temperature fluctuations and microscopic growth rates in a silicon floating zone under microgravity. J Cryst Growth 203:500
33. Lan CW, Chian JH (1999) Three-dimensional simulation of Marangoni flow and interfaces in floating-zone silicon crystal growth. J Cryst Growth 203:500
34. Selver R (2005) Experiments on the transition from the steady to the oscillatory marangoni convection of a floating-zone under various cold wall temperatures and various ambient air temperature effects. Microgravity Sci Technol 17:25
35. Rupp R, Müller G, Neumann G (1989) Three-dimensional time dependent modelling of the Marangoni convection in zone melting configurations for GaAs. J Cryst Growth 97:34
36. Kamotani Y, Matsumoto S, Yoda S (2007) Recent developments in oscillatory Marangoni convection. FDMP Fluid Dyn Mater Process 3:147

37. Cröll A, Kaiser T, Schweizer M, Danilewsky AN, Lauer S, Tegetmeier A, Benz KW (1998) Floating-zone and floating-solution-zone growth of GaSb under microgravity. J Cryst Growth 191:365
38. Nishinaga T, Ge P, Huo C, He J, Nakamura T (1997) Melt growth of striation and etch pit free GaSb under microgravity. J Cryst Growth 174:96
39. Tillberg E, Carlberg T (1990) Semi-confined Bridgman growth of germanium crystals in microgravity. J Cryst Growth 99:1265
40. Matthiesen DH, Wargo MJ, Motakef S, Carlson DJ, Nakos JS, Witt AF (1987) Dopant segregation during vertical Bridgman-Stockbarger growth with melt stabilization by strong axial magnetic-fields. J Cryst Growth 85:557
41. Kang J, Fukuda T (2000) Growth exploration of compositionally uniform bulk semiconductors under a high magnetic field of 80000 Gauss. Mater Sci Eng B 75:149
42. Yesilyurt S, Vujisic L, Motakef S, Szofran FR, Volz MP (1999) A numerical investigation of the effect of thermoelectromagnetic convection (TEMC) on the Bridgman growth of $Ge_{1-x}Si_x$. J Cryst Growth 207:278
43. Fripp AL, Debnam WJ, Rosch W, Chait A, Yao M, Szofran FR (2000) Melt stabilization of PbSnTe in a magnetic field. NASA Microgravity Mater Sci Conf
44. Cröll A, Szofran FR, Dold P, Benz KW, Lehoczky SL (1998) Floating-zone growth of silicon in magnetic fields II: strong static axial fields. J Cryst Growth 183:554
45. Baumgartl J, Müller G (1996) The use of magnetic fields for damping the action of gravity fluctuations (g-jitter) during crystal growth under microgravity. J Cryst Growth 169:582
46. Ma N, Walker JS (1997) Magnetic damping of buoyancy convection during semiconductor crystal growth in microgravity: spikes of residual acceleration. Phys Fluids 9:1182
47. Herrmann F, Müller G (1995) Growth of 20 mm diameter GaAs crystals by the Floating Zone technique with controlled as-vapour pressure under microgravity. J Cryst Growth 156:350
48. Fischer B, Friedrich J, Weimann H, Müller G (1999) The use of time-dependent magnetic fields for control of convective flows in melt growth configurations. J Cryst Growth 189:170
49. Barmin IV, Senchenkov AS, Greif A, Wunderwald U, Cröll A, Lyubimova T (2009) Application of rotating magnetic fields to crystal growth under microgravity (Experiments on Foton-M3). Magnetohydrodynamics 45:325
50. Feonychev A, Bondareva N (2002) Crystal growth under microgravity conditions with using of magnetic fields. In: 34th COSPAR scientific assembly, the second world space congress, Houston
51. Dold P, Benz KW (1997) Modification of fluid flow and heat transport in vertical Bridgman configurations by rotating magnetic fields. Cryst Res Technol 32:51
52. Lan CW, Tu CY (2002) Three-dimensional analysis of flow and segregation control by slow rotation for Bridgman crystal growth in microgravity. J Cryst Growth 237:1881
53. Lan CW (1999) Effects of ampoule rotation on flows and dopant segregation in vertical Bridgman crystal growth. J Cryst Growth 197:983
54. Lan CW (1999) Effects of centrifugal acceleration on the flows and segregation in vertical Bridgman crystal growth with steady ampoule rotation. J Cryst Growth 229:595
55. Churilov A, Ostrogorsky AG, Volz MP (2006) Solidification using a baffle in sealed ampoules: ground-based experiments. J Cryst Growth 295:20
56. Ostrogorsky AG (1990) Numerical simulations of single crystal growth by submerged heater method. J Cryst Growth 104:233
57. Ostrogorsky AG, Sell HJ, Scharl S, Müller G (1993) Convection and segregation during growth of Ge and InSb crystals by the submerged heater method. J Cryst Growth 128:201
58. Dutta PS, Ostrogorsky AG (1993) Segregation of tellurium in GaSb single crystals and associated diffusion coefficient in the solute layer. J Cryst Growth 197:749
59. Dutta PS, Ostrogorsky AG (2000) Segregation of Ga in Ge and InSb in GaSb. J Cryst Growth 217:360

60. Ostrogorsky AG, Marin C, Churilov A, Volz MP, Bonner WA, Duffar T (2008) Reproducible Te-doped InSb experiments in microgravity science glovebox at the International Space Station. J Cryst Growth 310:364
61. Ostrogorsky AG, Marin C, Volz MP, Duffar T (2009) Initial transient in Zn-dop ed InSb grown in microgravity. J Cryst Growth 311:3143
62. Cröll A, Volz MP (2009) Detached Bridgman growth—a standard crystal growth method with a new twist. MRS Bull 34:245
63. Yue JT, Voltmer FW (1975) Influence of gravity-free solidification on solute microsegregation. J Cryst Growth 29:329
64. Regel LL, Wilcox WR (1998) Detached solidification in microgravity—a review. Microgravity Sci Technol XI/4:152
65. Dold P, Szofran FR, Benz KW (2002) Detached growth of gallium doped germanium. J Cryst Growth 234:91
66. Schweizer M, Cobb SD, Volz MP, Szoke J, Szofran FR (2002) Defect density characterization of detached-grown germanium crystals. J Cryst Growth 235:161
67. Sylla L, Fauler A, Fiederle M, Duffar T, Dieguez E, Zanotti L, Zappettini A, Roosen G (2008) Dewetting during the crystal growth of (Cd, Zn)Te: in under microgravity. In: Nuclear science symposium conference record
68. Wang YZ, Regel LL, Wilcox WR (2000) Influence of contact angle, growth angle and melt surface tension on detached solidification of InSb. J Cryst Growth 209:175
69. Duffar T, Dusserre P, Picca F, Lacroix S, Giacometti N (2000) Bridgman growth without crucible contact using the dewetting phenomenon. J Cryst Growth 211:434
70. Palosz W, Volz MP, Cobb S, Motakef S, Szofran FR (2005) Detached growth of germanium by directional solidification. J Cryst Growth 277:104
71. Sangiorgi R, Muolo ML, Chatain D, Eustathopoulos N (1988) Wettability and work of adhesion of nonreactive liquid metals on silica. J Am Ceram Soc 71:742
72. Kaiser N, Cröll A, Szofran FR, Cobb SD, Volz M, Dold P, Benz KW (2001) Determination of wetting angles of germanium melts using the sessile drop technique. J Cryst Growth 231:448
73. Zemskov VS, Raukham MR, Barnim IV, Senchenkov AS, Shulpina IL, Sorokin LM (1983) Special features of solidification of alloyed single crystals of indium antimonide in zero gravity conditions. Fizika i Khimiya Obrabotky Materialov 17:56
74. Tegetmeier A (1995) Oberflächenspannung und Wachstumswinkel, zwei wichtige Parameter der Schmelzzonenzüchtung. Dissertation thesis, AlbertLudwigs- Universität
75. Shetty R, Balasubramanian R, Wilcox WR (1990) Surface tension and contact angle of molten semiconductor compounds: I. Cadmium telluride. J Cryst Growth 100:51
76. Mukai K, Yuan Z (2000) Wettability of ceramics with molten silicon at temperatures ranging from 1693 K to 1773 K. Mater Trans JIM 41:338
77. Duffar T, Abadie J (1996) Wetting of InSb melts on crucibles in weightlessness—results of the Texus 32/TEM 01–4 experiment. Microgravity Sci Technol IX
78. Harter I, Dusserre P, Duffar T, Nabot J-P, Eustathopoulos N (1993) Wetting of III–V melts on crucible materials. J Crys Growth 131:157
79. Wald FV (1981) Crystals: growth, properties and applications, vol 5. Springer, New York
80. Fiederle M, Duffar T, Garandet JP, Babentsov V, Fauler A, Benz KW, Dusserre P, Corregidor V, Dieguez E, Delaye P, Roosen G, Chevrier V, Launay JC (2004) J Cryst Growth 267:429
81. Yeckel A, Stelian C, Derby JJ (2009) Heat transfer, capillarity, and phase change during detached Bridgman crystal growth. In: Thermodynamics of phase changes (EUROTHERM-84), Namur, Belgium
82. Yeckel A, Daoutidis P, Derby JJ (2012) Stabilizing detached Bridgman melt crystal growth: proportional-integral feedback control. J Cryst Growth 356:33
83. Yeckel A, Daoutidis P, Derby JJ (2012) Stabilizing detached Bridgman melt crystal growth: model-based nonlinear feedback control. J Cryst Growth 361:16

84. Szofran FR, Cobb SD, Cröll A, Dold P, Kaiser N, Kerat U, Benz KW, Motakef S, Volz MP, Schweizer M, Vujisic L, Walker JS, Pettigrew P (2000) Reduction of defects in germanium-silicon (RDGS). In: NASAMSFC, Huntsville, AL, Science Requirements Document (SRD), 19–20 December 2000
85. Duffar T, Dusserre P, Giacometti N (2001) Growth of GaSb single crystals by an improved dewetting process. J Crys Growth 223:69
86. Mauk MG, Andreev VM (2003) GaSb-related materials for TPV cells. Semicond Sci Tehnol 18:S191
87. Wang XW, Lee H, Lan YC, Zhu GH, Joshi G, Wang DZ, Yang J, Muto AJ, Tang MY, Klatsky J, Song S, Dresselhaus MS, Chen G, Ren ZF (2008) Enhanced thermoelectric figure of merit in nanostructured n-type silicon germanium bulk alloy. Appl Phys Lett 93:193121
88. Kinoshita K, Yoda S (2011) Growth of homogeneous semiconductor mixed crystals by the traveling liquidus-zone method. J Cryst Growth 318:1026
89. Kinoshita K, Ogata Y, Adachi S, Koshikawa N, Yoda S (2005) Excellent compositional homogeneity in In0.3Ga0.7As crystals grown by the traveling liquids-zone (TLZ) method. Microgravity Sci Technol 16:71
90. Kinoshita K et al (2015) Growth of 2 inch $Si_{0.5}Ge_{0.5}$ bulk single crystals. Jpn J Appl Phys 54:04DH03
91. Kinoshita K et al (2012) Homogeneous $Si_{0.5}Ge_{0.5}$ bulk crystal growth as substrates for strained Ge thin films by the traveling liquidus-zone method. Thin Solid Films 520:3279
92. Kinoshita K et al (2011) Homogeneous SiGe crystal growth in microgravity by the travelling liquidus-zone method. J Phys Conf Ser 327:012017
93. Konoshita K et al (2015) Compositional uniformity of a $Si_{0.5}Ge_{0.5}$ crystal grown on board the International Space Station. J Cryst Growth 419:47
94. Abe K et al (2014) Numerical simulations of SiGe crystal growth by the traveling liquidus-zone method in a microgravity environment. J Cryst Growth 402:71
95. Tsuruta T, Hayakawa Y, Kumagawa M (1988) Effect of ultrasonic vibrations on the growth of $In_xGa_{1-x}Sb$ mixed-crystals. Jpn J Appl Phys 27:47
96. Tsuruta T, Hayakawa Y, Kumagawa M (1989) Effect of ultrasonic vibrations on the growth of $In_xGa_{1-x}Sb$ mixed-crystals (ii). Jpn J Appl Phys 28:36
97. Tsuruta T et al (1992) Effect of ultrasonic vibrations on the growth of $In_xGa_{1-x}Sb$ mixed-crystals (iii). Jpn J Appl Phys 31:23
98. Tanaka A et al (2000) Multi-step pulling of GaInSb bulk crystal from ternary solution. J Cryst Growth 209:625
99. Dutta PS, Ostrogorsky AG (1998) Suppression of cracks in $In_xGa_{1-x}Sb$ crystals through forced convection in the melt. J Cryst Growth 194:1
100. Kozhemyakin GN (2000) Indium inhomogeneity in $In_xGa_{1-x}Sb$ ternary crystals grown by floating crucible Czochralski method. J Cryst Growth 220:239
101. Stelian C et al (2005) Growth of concentrated GaInSb alloys with improved chemical, homogeneity at low and variable pulling rates. J Cryst Growth 283:124
102. Stelian C et al (2004) Solute segregation in directional solidification of GaInSb concentrated alloys under alternating magnetic fields. J Cryst Growth 266:207
103. Stelian C et al (2005) Bridgman growth of concentrated GaInSb alloys with improved compositional uniformity under alternating magnetic fields. J Cryst Growth 275:E1571
104. Yu D et al (2016) A review on InGaSb growth under microgravity and terrestrial conditions towards future crystal growth project using Chinese Recovery Satellite SJ-10. Microgravity Sci Technol 28:143
105. Murakami N et al (2008) Growth of homogeneous InGaSb ternary alloy semiconductors on InSb seed. J Cryst Growth 310:1433
106. Hayakawa Y et al (2008) In situ observation of composition profiles in the solution by X-ray penetration method. J Cryst Growth 310:1487

107. Rajesh G et al (2010) In-situ observations of dissolution process of GaSb into InSb melt by X-ray penetration method. J Cryst Growth 312:2677
108. Sakata K et al (2014) Thermal properties of molten InSb, GaSb, and $In_xGa_{1-x}Sb$ alloy semiconductor materials in preparation for crystal growth experiments on the International Space Station. Adv Space Res 53:689
109. Inatomi Y et al (2015) Growth of $In_xGa_{1-x}Sb$ alloy semiconductor at the International Space Station (ISS) and comparison with terrestrial experiments. npj Microgravity 1:15011
110. Kumar N et al (2016) Investigation of directionally solidified InGaSb ternary alloys from Ga and Sb faces of GaSb(111) under prolonged microgravity at the International Space Station. npj Microgravity 2:16026
111. Kazuhiko O et al (1997) Melt mixing of the 0.3In/0.7GaSb/0.3Sb solid combination by diffusion under microgravity. Jpn J Appl Phys 36:3613
112. Mirsandi H et al (2015) A numerical study on the growth process of InGaSb crystals under microgravity with interfacial kinetics. Microgravity Sci Technol 27:313–320